

Optically Controlled Nano-Transducers Based on Cleaved Superlattices for Monitoring Gigahertz Surface Acoustic Vibrations

Changxiu Li, Nikolay Chigarev, Théo Thréard, Kedong Zhang, Nicolas Delorme, Vincent Tournat, Samuel Raetz, Hong Lu, and Vitalyi E. Gusev*



Cite This: <https://doi.org/10.1021/acsnano.3c07576>



Read Online

ACCESS |

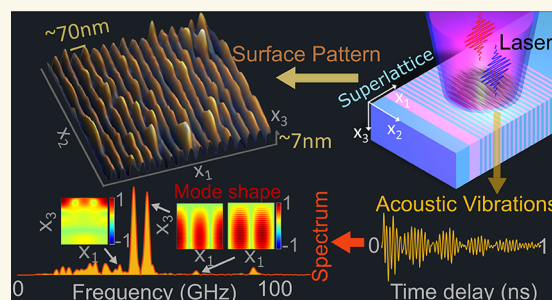
Metrics & More

Article Recommendations

Supporting Information

ABSTRACT: Surface acoustic waves (SAWs) convey energy at subwavelength depths along surfaces. Using interdigital transducers (IDTs) and opto-acousto-optic transducers (OAOTs), researchers have harnessed coherent SAWs with nanosecond periods and micrometer localization depth for various applications. These applications include the sensing of small amount of materials deposited on surfaces, assessing surface roughness and defects, signal processing, light manipulation, charge carrier and exciton transportation, and the study of fundamental interactions with thermal phonons, photons, magnons, and more. However, the utilization of cutting-edge OAOTs produced through surface nanopatterning techniques has set the upper limit for coherent SAW frequencies below 100 GHz, constrained by factors such as the quality and pitch of the surface nanopattern, not to mention the electronic bandwidth limitations of the IDTs. In this context, unconventional optically controlled nanotransducers based on cleaved superlattices (SLs) are here presented as an alternative solution. To demonstrate their viability, we conducted proof-of-concept experiments using ultrafast lasers in a pump–probe configuration on SLs made of alternating $\text{Al}_x\text{Ga}_{1-x}\text{As}$ and $\text{Al}_y\text{Ga}_{1-y}\text{As}$ layers with approximately 70 nm periodicity and cleaved along their growth direction to produce a periodic nanostructured surface. The acoustic vibrations, generated and detected by laser beams incident on the cleaved surface, span a range from 40 to 70 GHz, corresponding to the generalized surface Rayleigh mode and bulk modes within the dispersion relation. This exploration shows that, in addition to SAWs, cleaved SLs offer the potential to observe surface-skimming longitudinal and transverse acoustic waves at GHz frequencies. This proof-of-concept demonstration below 100 GHz in nanoacoustics using such an unconventional platform might be useful for realizing sub-THz to THz coherent surface acoustic vibrations in the future, as SLs can be epitaxially grown with atomic-scale layer width and quality.

KEYWORDS: surface and surface skimming acoustic waves, superlattices, opto-acousto-optic transducers, nanoacoustics, picosecond laser ultrasonics, coherent GHz phonons, ultrafast laser spectroscopy



Surface acoustic waves (SAWs) possess the distinct ability to interact with various state variables within solids. These variables include electrons, spins, photons, magnons, thermal phonons, and strain, enabling the evaluation and/or modification of material properties at subwavelength depths near the surface. The significance of SAWs spans over six decades, beginning with the invention of interdigital transducers (IDTs) in 1965¹ and their subsequent use in combination with lasers for SAW monitoring in 1968.² While lower-frequency SAWs, falling within the ultrasonic range, have been influential in communication and signal processing technologies,³ higher-frequency SAWs have found applications in diverse fields. These application include material characterization,⁴ photonic modulation,^{5,6} optomechanics,⁷ the transport of other excitations,^{8–10} and interactions with magnons.¹¹

SAWs are involved in a variety of products for information and communication technologies (ICTs), including mobile devices (utilized in central processing units, signal converters and gyroscopes) and devices associated with the “Internet of Things”, where they find applications in sensors and integrated energy converters.

Received: August 13, 2023

Revised: March 5, 2024

Accepted: March 8, 2024

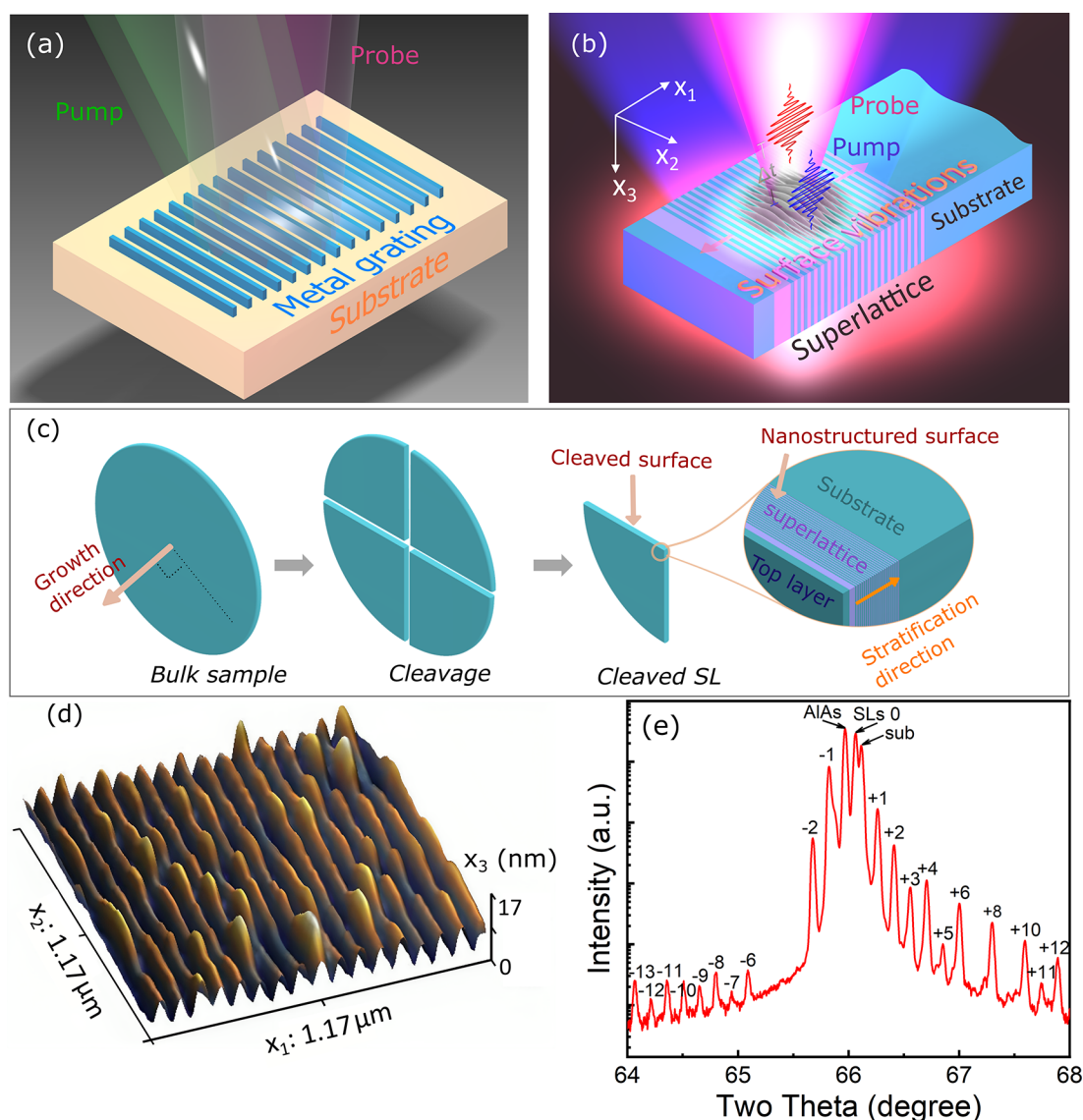


Figure 1. (a) An illustrative display of a metal grating structure. (b) Schematic of pump–probe experiments on the cleaved SL. (c) The illustration of the experimental sample preparation. GaAs substrate with the grown on it SL and cap GaAs layer is denoted as bulk sample. (d) AFM image of a cleaved GaAs/AlAs SL surface modified by oxidation. (e) X-ray diffraction measurement of a GaAs/AlAs SL.

At present, the upper operational frequency limit for coherent SAWs controlled by IDTs or opto-acousto-optic transducers (OAOTs) remains below 100 GHz.^{12,13} Extending this frequency range to subterahertz (sub-THz) range in integrated elasto-optic modulators and SAW processors/filters holds significant potential for future ICT devices. Access to higher frequencies and broader channel bandwidths is considered essential for the continued expansion of global mobile communications. Sub-THz SAWs could provide the means to characterize materials at depths in the single-digit nanometer range beneath the surface. They could be also applied to characterize materials or molecules deposited between the SAW emitter and detector along the path of SAW propagation. A primary objective of an ongoing research is to develop techniques for exciting and detecting coherent SAWs with picosecond periods and deeply suboptical, nanometer-scale wavelengths and localization depths for applications in nanometrology, nanoimaging, as well as in sensing and manipulations for both fundamental and applied research and the field of ICTs.

From a theoretical perspective, the generation of SAWs at a specific frequency necessitates the creation of a spatiotemporal stress distribution in a material at the SAW penetration depth during excitation. The temporal Fourier spectrum of this distribution should include the desired frequency component. Simultaneously, its spatial Fourier spectrum along the surface should encompass the required SAW wavenumbers.¹⁴ The expansion of IDTs to sub-THz frequencies faces limitations due to electronics bandwidth, unlike laser-based methods, which lack such restrictions. Intensity envelopes of laser pulses lasting less than a picosecond contain frequencies up to the terahertz range, effectively incorporating these frequencies into the spectrum of photoinduced stress.

Creating the required high wavenumbers in the spatial distribution of photoinduced stress can be accomplished using laser gratings. This technique involves the interference between two overlapping laser beams propagating at an angle, forming an intensity pattern with periodicity that selects the SAW wavenumber.^{15–17} In this technique, the ratio of the wavevector of SAW to that of electromagnetic radiation is less

than or equal to 2.^{17,18} Notably, in laser methods, SAWs are detected by observing the scattering of probe laser radiation due to SAW-induced changes in the material refractive index and/or the surface topography. The highest-frequency Rayleigh SAW (50 GHz) was generated and detected using extreme ultraviolet (EUV) light grating with an 84 nm period.¹⁸ Femtosecond pump pulses at a wavelength of 39.9 nm and a probe pulse at a wavelength of 13.3 nm were derived from the FERMI free electron laser source. EUV radiation from the free electron laser was also employed to induce gratings with a minimum period of 28 nm, although this allowed monitoring of only the longitudinal acoustic waves propagating along the grating direction.¹⁹ Due to the very high velocities of the longitudinal waves in the sample, the 28 nm EUV gratings provided the capability to monitor longitudinal acoustic waves up to 360 GHz in frequency.

As an alternative, the nanometer spatial periodicity of laser-induced stresses can be achieved through surface nanostructuring. Historically, material nanopatterning has been accomplished through depositing nanoscale arrays of metal lines (Figure 1a). In these cases, SAWs were predominantly generated via the thermoelastic stress induced by laser heating of such grating.^{20,21} Experiments with metallic gratings having a minimum period of around 40 nm were conducted using 800 nm infrared pump laser pulses and 30 nm EUV probe laser pulses.²² The highest reported coherent SAW frequency was approximately 90 GHz, achieved in 100 nm period metallic gratings pumped and probed using near-infrared light (at around 820 nm wavelengths),¹³ indicating successful generation and detection with deeply suboptical gratings.

However, for SAWs to reach 1 THz, the grating period controlling the wavenumber should be shorter than 3 nm, assuming a typical Rayleigh SAW velocity of 3000 m/s in the material. The minimum period of structures currently patterned in leading research laboratories is around 10 nm.^{23–25} Therefore, the primary limitation in generating SAWs at frequencies near 1 THz is the need to reduce surface nanopatterning pitch while improving its quality. We propose that this limitation can be addressed by engineering unconventional OAOTs based on cleaved nanostructured bulk materials. Bulk superlattices (SLs) with a period of several atomic layers and atomic-scale quality at the interfaces can currently be grown by epitaxy. These SLs can be cleaved or sliced (i.e., with microtome) along the surface normal to their layering, producing a nanopatterned surface, with the periodicity and quality of bulk samples, that can control SAWs (Figure 1b). Figure 1c depicts the consecutive steps of a cleaved SL attainment from a bulk SL grown on a substrate through cleavage. While the highest frequencies of coherent bulk acoustic waves up to 3 THz have been generated and detected by lasers in SLs/multiple quantum well structures,^{26,27} they have not yet been applied to control SAWs. Previously, the cleaved SL structure was theoretically investigated.²⁸ This structure is stratified normal to the cleaved surface and has physical parameters varying periodically not only in the bulk but also at its cleaved mechanically free surface. It was studied as a SAW phononic crystal, and an increased efficiency of the optoacoustic (OA) conversion in cleaved semiconductor SL for monitoring GHz SAWs was suggested.^{29,30} Note that we will henceforth refer to the experimental SL structure with notation “SL stratified normal to the surface”, as suggested in the pioneering theoretical investigation.²⁸ While the theoretical investigations were conducted more than three decades ago,

experimental demonstrations of acoustic waves on such nanostructures have not yet been realized. Here, on the platform of cleaved semiconductor SLs, we conducted proof-of-concept experiments for all-optical monitoring of coherent acoustic vibrations of the surface (Figure 1b), encompassing various acoustic modes, including generalized Rayleigh-type (gR) surface acoustic waves, surface-skimming transversal (T), and longitudinal (L) acoustic waves, all of which are reported within this work. Two samples have been tested. The first, an GaAs/AlAs SL with a 71 nm period, allowed us to simultaneously monitor the gR, T, and L waves at frequencies of 40.2, 50.9, and 70.3 GHz, respectively, using near-infrared femtosecond lasers. In the second sample, containing two Al_{0.2}Ga_{0.8}As/Al_{0.4}Ga_{0.6}As SLs of the same period but with a modified content of Al in constituent layers compared to the first sample, the gR wave at 40 GHz frequencies was also monitored.

RESULTS AND DISCUSSION

The nanostructures were prepared by epitaxial growth along the (001) direction of a semiconductor SL on a GaAs substrate, layer by layer, with precise control of each layer composition (alternating between Al_xGa_{1-x}As and Al_yGa_{1-y}As) and thickness (alternating between d_1 and d_2). This growth resulted in a periodic stack of nanometers-thin layers stratified normal to the substrate surface. Two semiconductor structures were investigated. They contain SLs with a nominally equal period and individual layer thickness of $d_{\text{SL}} = 71.4$ nm, $d_1 = 40.0$ nm, $d_2 = 31.4$ nm, while the constituent materials are GaAs/AlAs and Al_{0.2}Ga_{0.8}As/Al_{0.4}Ga_{0.6}As, respectively. The first sample contains a single SL of 5.35 μm thickness, and the second one contains two SLs of 1.2 μm thickness separated by a 1 μm thick GaAs layer. Cleavage procedures were applied to the sample along the growth direction, perpendicular to the substrate surface, producing a mirror-finished nanostructured surface for optical monitoring of coherent acoustic phonons (Figure 1b).

However, oxidation of Al_xGa_{1-x}As ($x \neq 0$) layers exposed to air occurred. The morphology of the nanostructured surface two months after cleavage was revealed by atomic force microscopy (AFM, see Methods A), showing ripples with a periodicity of 71 nm, extracted from a 2D FFT analysis of the image. Apart from local defects, the average modulation depth of the oxidation induced ripples is 7 nm in the GaAs/AlAs SL (see Figure 1d). Therefore, the sample with the nanostructured surface (Figure 1c) was freshly cleaved just before the pump–probe experiments to minimize oxidation effects, although complete prevention was not achieved.

It is worth noting that in the second sample, the Al content is sufficiently low in both SL layers to significantly reduce the surface oxidation effect.³¹ The X-ray diffraction (XRD) results on the GaAs/AlAs SL confirmed the good quality and periodicity of the structure (see Figure 1e and Methods A). In contrast to a metal grating deposited on a substrate (see Figure 1a), the cleaved SL structures (Figure 1b) acquire their nanopatterned surface through the nanostructuring of bulk SLs. Common techniques such as lithography and focused ion beam are employed for nanostructuring only the surface.

The periodicity of the mechanical/acoustical properties (such as density and elastic moduli) in the cleaved SLs gives rise to Brillouin zone-center acoustic eigenmodes with corresponding lateral, i.e., along x_1 direction on the cleaved surface, periodicity of the mechanical strain/displacement

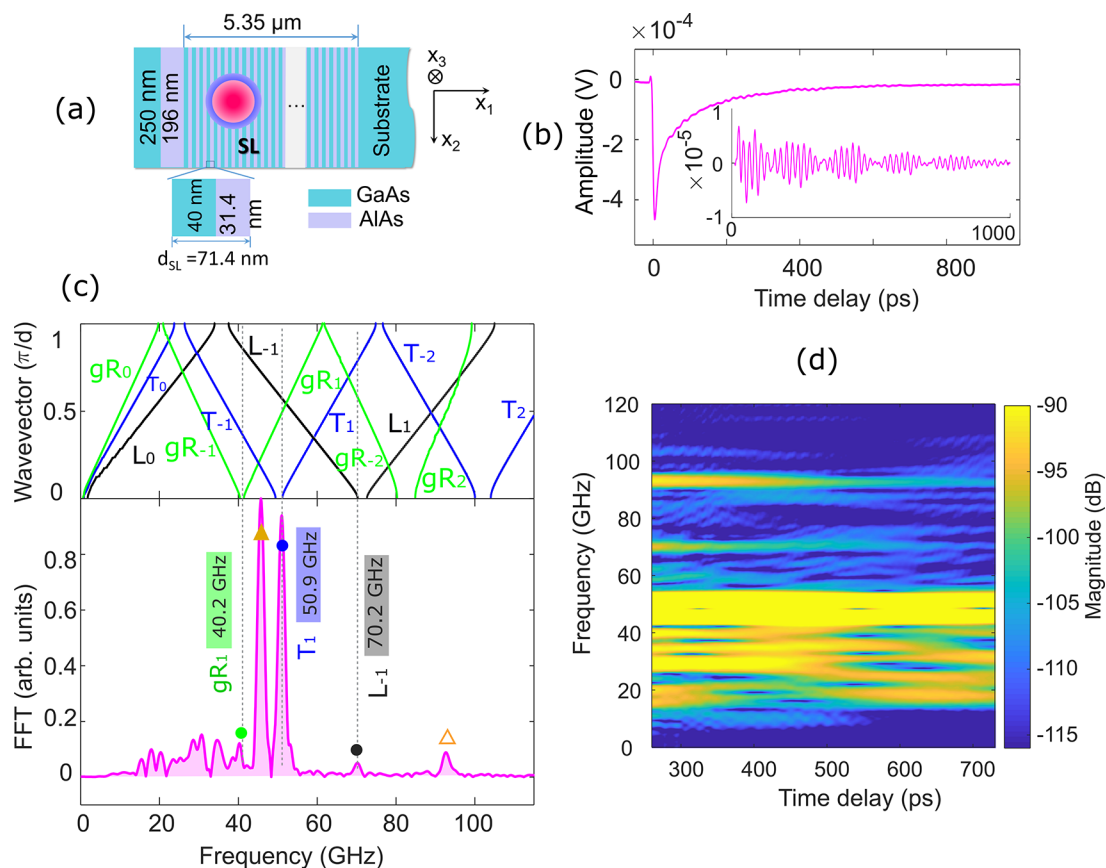


Figure 2. Presentation of the scheme and of evaluation results for the first sample. (a) Schematic depiction of the sample surface and of a potential laser focus position. (b) Time-domain reflectivity signal. Inset: acoustically induced oscillations in the transient reflectivity signal after removing nonoscillating background. (c) Upper part: calculated dispersion relations of acoustic modes in the SL, which is infinitely thick along x_1 and semi-infinite along x_3 (green, gR; blue, T; black, L). Subscripts indicate acoustic band orders; lower part: spectrum of the acoustic vibrations presented in the inset of (b). Green, blue, and black solid dots indicate the identified first-order $k_1 = 0$ gR, T, and L waves, respectively. Brown solid and hollow triangles represent the frequencies of bulk longitudinal acoustic waves propagating in the zeroth (45.7 GHz) and first (92.6 GHz) diffraction orders, respectively. (d) Spectrogram of the acoustic signal shown in the inset of part (b) obtained by short-time Fourier transform (see Methods F for details).

fields. These modes, for example, gR waves, contain lateral unmodulated/homogeneous components, which correspond to infinitely long modulation period (see Methods B). The same lateral periodicity of the optical properties, i.e., of the complex optical refractive index, significantly enhances the possibilities for optically generating these acoustic eigenmodes (see Methods C). The identical periodicity of both optical and acousto-optical properties, i.e., of the complex photoelastic tensor, facilitates the optical detection of these modes (see Methods D).

It is important to note that the existence of laterally unmodulated and homogeneous eigenmode components is theoretically advantageous for their all-optical monitoring. High-frequency acoustic modes at the zone center can be excited even by the laterally homogeneous part of the distributed photoinduced stresses acting on laterally homogeneous components in the mode structure. These modes can be detected through time-domain backward Brillouin scattering of the normally incident probe light, even when the SL motion is laterally unmodulated, meaning that scattering occurs from the motion of the SL averaged over its period (see Methods C and D). Due to the short periodicity in their physical properties, the designed SLs stratified normal to the surface (x_1x_2 plane in Figure 1b)²⁸ offer the opportunity to optically monitor surface

acoustic vibrations with deeply suboptical lateral periodicity because they are composed of the acoustic waves with deeply suboptical lengths.

We conducted ultrafast pump–probe transient reflectivity experiments to monitor coherent acoustic phonons on the cleaved SL surface of the prepared samples (see Figure 1b and Methods A). Unlike the conventional setup for monitoring bulk acoustic waves in SLs,²⁶ where the pump and the probe laser beams are incident on the plane x_2x_3 , in this case, they are directed normally to the cleaved plane x_1x_2 . Laser wavelengths of 405 nm/810 nm were chosen for the pump and probe laser beams, which were collinearly cofocused by a 100× objective onto the sample, creating a spot with a radius of approximately 0.82 μm (measured at $1/e^2$ by cross-correlation, see Methods E for details). We monitored the time-dependent reflectivity change of the sample, induced by the pump excitation on the cleaved structure, using the probe light whose intensity was modulated by this change, and we captured it with a photodetector.

The experimental results obtained from both SL-based structures are now presented and compared favorably with theoretical expectations. The proof-of-concept experiment was conducted on the first sample, which was based on the cleaved 5.35 μm thick GaAs/AlAs SL. In this configuration, the laser

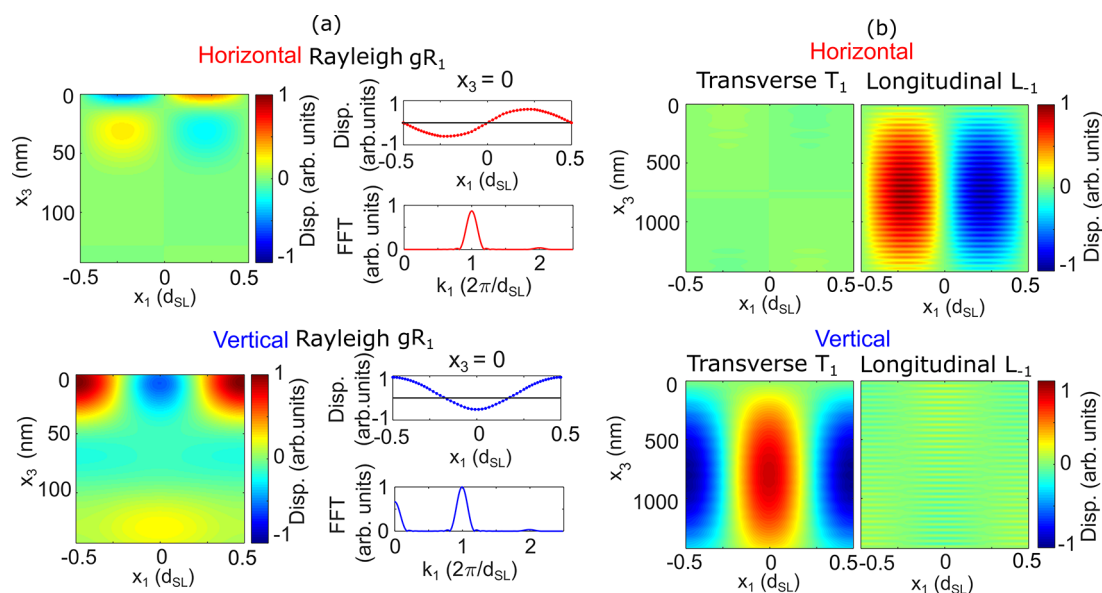


Figure 3. Calculated spatial distributions of the mechanical displacement components in the first-order zone center $k_1 = 0$ symmetric (a) gR (41.4 GHz), (b) T (51.2 GHz), and L (70.3 GHz) acoustic modes. Disp. denotes displacement. The second column in (a) presents the displacements at mechanically free surface and their k_1 spectra, highlighting the presence of the spatially homogeneous component in the gR mode structure.

beams were focused entirely on the SL region (see Figure 2a). The interband absorption of the pump laser pulses in the GaAs creates electron–hole pairs, whose distribution dominantly contributes to the generation of acoustic waves through the stress induced by the electron hole–phonon deformation potential mechanism.³² Notably, this opto-acoustic conversion mechanism is much more efficient than the thermo-elastic one, most commonly found in metallic grating OA transducers.^{13,14} The reflectivity change induced by the acoustic waves (phonons) is monitored by the probe near-infrared light as a function of the time delay between the pump and the probe pulses.

The time-domain signal (Figure 2b, main part) reveals that the acoustically induced oscillations (Figure 2b, inset) are superimposed on the monotonous exponential variations in amplitude caused by the generation/recombination of the electron–hole pairs and transient heating of the sample after photoexcitation. To enhance the display of acoustic oscillations (Figure 2b, inset), the dominant background is numerically removed, following the signal processing details in Methods F. Due to the SL periodicity, the projections k_1 of the wave vectors on x_1 axis, which are larger than π/d_{SL} in the acoustic modes dispersion relations, are folded into a mini-Brillouin zone (see Figure 2c, upper section, and Methods G for details on numerical calculations). In this zone, the gR , T , and L waves differ in frequencies due to the differences in their propagation velocities. The gR waves become supersonic above the frequency corresponding to the intersection of the first-order optical surface phonon branch R_{-1} and the bulk acoustical phonon branch T_0 , leading to attenuation through the emission of bulk acoustic waves (Brekhovskich attenuation).³³

However, due to the small relative differences between the parameters of the SL constituent materials, $\mu \ll 1$, where μ represents the ratios of parameter differences to average parameter values, such as $\Delta C_{11}/\langle C_{11} \rangle = 0.0117$, $\Delta C_{12}/\langle C_{12} \rangle = 0.058$, $\Delta C_{44}/\langle C_{44} \rangle = 0.00845$ and $\Delta \rho/\langle \rho \rangle = 0.33668$ for GaAs/AlAs, a basic analysis (see Supporting Information, S1)

demonstrates that the $k_1 = 0$ gR wave experiences a slight frequency shift and a weak attenuation proportional to μ^2 ($\Delta \text{Re}(\omega_{gR})/\omega_{gR} \sim \mu^2$, $\text{Im}(\omega_{gR})/\omega_{gR} \sim \mu^2$, with ω denoting the cyclic frequency). The numerical simulations of the eigenmode dispersion relations in the laterally infinite cleaved SL shown in the upper panel of Figure 2c, enable the identification of three peaks. These peaks, found in the experimental spectrum in the lower section of Figure 2c at frequencies 40.2, 50.9, and 70.2 GHz, correspond to the zone center vibrational motions induced by the gR , T , and L waves, respectively. Figure 2d depicts the spectrogram of the acoustic signal in Figure 2b and shows how the frequency contents of the signal vary with time delay. This will be further discussed later on.

Figure 3 illustrates the calculated shapes of these three modes, revealing that the vibrations caused by the gR wave (Figure 3a) are highly localized near the surface (at depths smaller than one SL period). In contrast, the vibrations induced by the T and L waves (Figure 3b) are nonlocalized. To better appreciate the surface displacement at $x_3 = 0$ induced by the gR wave, the horizontal (top) and vertical (bottom) displacement are displayed in the second column of Figure 3a as a function of x_1 . It is important to note here that both components depict spatial periodicity associated with the SL periodicity d_{SL} . More importantly, the vertical component, unlike the horizontal one, contains a nonzero mean value as seen from the nonzero surface area and, related nonzero Fourier component at $k_1 = 0$ of its displacement distribution. The differences in amplitude of the related transient reflectivity oscillations between the gR and T waves at closely matched frequencies can likely be attributed to the oxidation of AlAs layers and the imperfect cleavage procedures, which introduce surface defects and roughness (as shown in Figure 1d). These factors are expected to exert a more significant influence on the generation, propagation, and detection of surface-localized acoustic eigenmodes compared to their delocalized counterparts.

The two additional peaks present in the experimental spectrum in Figure 2c at frequencies of 45.7 and 92.6 GHz can

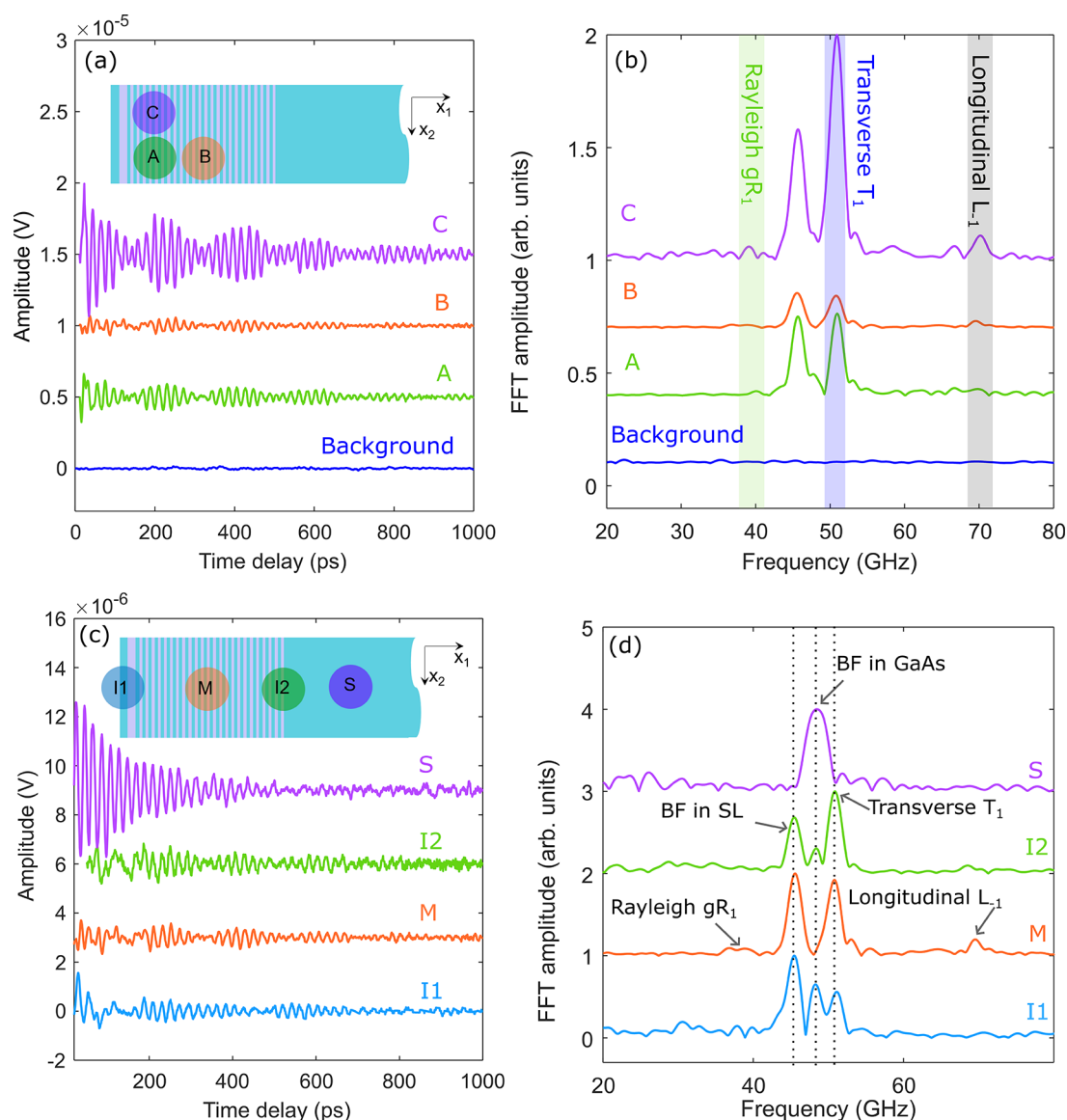


Figure 4. Experimental measurements on the first sample. (a) Detection of acoustic vibrations and (b) their spectra obtained by overlapping the pump and probe foci at positions A, B, and C on the SL. These results are compared with background measurements (zero pump light). In (b) the spectral components attributed to the gR, T, and L waves are highlighted in color. (c) Detection of acoustic vibrations and (d) their spectra achieved by overlapping pump/probe foci at positions I1, M, I2, S on top layer/SL interface, SL, SL/GaAs interface, and substrate, respectively. The three spectral peaks indicated by vertical dotted lines correspond to the Brillouin frequency (BF) in the SL (45 GHz, left), the BF in GaAs (48 GHz, middle), and the frequency of the T wave in the SL (51 GHz, right), respectively.

be attributed to the Brillouin frequencies induced by the probe light that is backward scattered by the coherent bulk acoustic modes launched within the bulk (i.e., depth) of the SL nanostructure by the pump laser radiation. This is detailed in Methods H, where we derive the analytical estimates of Brillouin frequencies for light scattering by quasi-longitudinal acoustic (QLA) waves propagating in the diffraction orders $n = 0$ and $n = 1$, respectively.

Several spectral components below 40 GHz, not consistently replicable in the experiments, are likely attributable to random noise originating from the optical system or electronic devices. However, it is not within the scope of this discussion to delve further into those frequencies due to their low repeatability.

To assess the reliability and variations in the monitored signals, we adjusted the laser foci laterally and vertically on the cleaved surface. We conducted these adjustments at positions

labeled A, B, and C within the SL region (as shown in Figure 4a,b). Here, we aim to replicate the vibrations induced by the gR, T, and L waves at their anticipated frequencies. However, it is noteworthy that the amplitudes of these vibrations exhibit variations based on the specific positions due to the inherent inhomogeneities within the SL material, as depicted in Figure 1d. Furthermore, these results are compared with the background measurements, and these comparisons indicate that the noise level, approximately at 10^{-7} , remains consistently below the level of the identified folded acoustic phonons.

It is also enlightening to shift the lateral position of the laser foci across different regions, encompassing the top layer/SL interface (I1), the SL itself (M), the SL/GaAs interface (I2), and the substrate (S) (refer to Figure 4c,d). By demarcating three prominent peaks with vertical dotted lines, we uncover that the middle frequency at 48 GHz is notably absent when

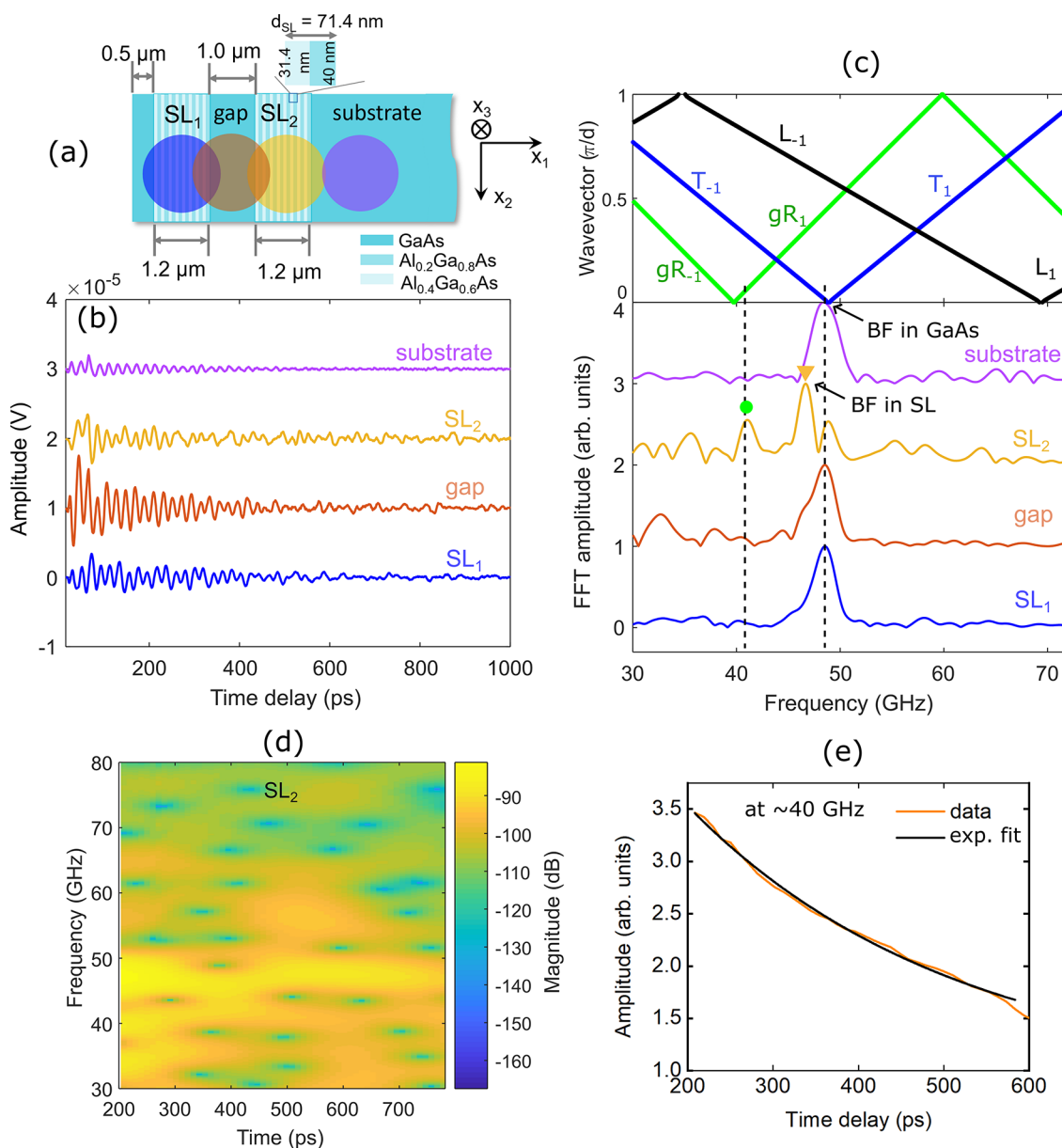


Figure 5. Presentation of the scheme and of the evaluation results for the second sample. (a) Schematic depiction of the sample surface and of the laser foci positions tested on SL₁, gap, SL₂, and substrate. (b) Contributions to transient reflectivity signal induced by acoustic vibrations. (c) Upper part: computed dispersion relations of acoustic modes in the SLs, considered to be laterally infinite along x_1 and semi-infinite along x_3 (green, gR; blue, T; black, L); lower part: spectra of acoustic vibrations shown in (b). (d) Spectrogram of the acoustic signal on SL₂ shown in part (b) obtained by short-time Fourier transform (see Methods F for details). (e) Attenuation of 40 GHz mode as a function of the time delay, extracted from (d).

probing at position M within the SL. However, this frequency is present at interfaces I1 and I2, and corresponds to the Brillouin frequency detected in the GaAs substrate at position S. This observation affirms our expectations that the Brillouin frequency measured within the SL does not coincide with that in the GaAs substrate. The Brillouin frequency at 45 GHz (represented by the left dotted line) detected within the SL region exhibits a red-shift relative to the Brillouin frequency in the GaAs, primarily due to the SL lower refractive index compared to the bulk GaAs when considering the probe light wavelength. The frequency at 51 GHz (as indicated by the right dotted line) is detected at all positions except the substrate, hinting at its origin as a folded acoustic mode arising from the nanostructure periodicity. Additionally, other folded

coherent acoustic modes are partially detected at the interfaces (as seen in the comparison between parts b and d of Figure 4).

Finally, we investigated the excitation and detection of surface modes on the second sample. A lateral scan of overlapping pump and probe laser beams was conducted on the sample containing the two Al_{0.2}Ga_{0.8}As/Al_{0.4}Ga_{0.6}As SLs (Figure 5a). It is worth noting that the individual thicknesses of SL₁, SL₂, and the gap are smaller than the focused beam spot. Consequently, the light is always partially absorbed by GaAs when directed at the SLs.

The spectral peak at 48.5 GHz is identified as the Brillouin frequency in the GaAs substrate when the laser foci do not overlap with the SL (purple spot in Figure 5a). However, at the three other positions, a potential contribution to this spectral

peak from the T wave, theoretically predicted at 49 GHz (see the upper part of Figure 5c) cannot be ruled out.

In SL₂, we monitor the folded first-order $k_1 = 0$ gR wave frequency at 41 GHz (indicated by the green solid dot) along with the Brillouin frequency at 46.6 GHz. The absence of these frequency components on the SL₁ can be attributed to a nonideal surface quality or SL quality at the sample edge (there is only 500 nm distance between the top layer/air interface and SL₁ left edge).

The peak at about 40 GHz, attributed to the gR mode, exhibits an exponential decay with a lifetime τ_s of approximately 300 ps, obtained from the exponential fit, shown in Figure 5e, of the amplitude attenuation with time delay at 40 GHz extracted from the spectrogram in Figure 5d. This gR wave lifetime is comparable to that shown in Figure 2d. The propagation velocity of the gR wave can be estimated as $v_{\text{gR}} \equiv d_{\text{SL}}\omega_{\text{gR}}/2\pi \cong 2930$ m/s. The escape time τ_a of the gR wave from the region where it is monitored, defined by the laser foci radius a , can be estimated as $\tau_a \equiv 2a/v_{\text{gR}} \approx 550$ ps. Therefore, it is not just the escape time that limits the observed lifetime τ_s of the gR wave signal. The gR wave lifetime τ_{gR} potentially limited by gR wave diffraction, its absorption in the bulk of the materials due to inelastic processes, its scattering by surface roughness, and emission of the bulk acoustic waves, can be estimated from the relation $\tau_s^{-1} = \tau_a^{-1} + \tau_{\text{gR}}^{-1}$, as $\tau_{\text{gR}} \approx 660$ ps. The diffraction time of the gR wave, τ_D , can be estimated as $\tau_D \sim (2a)^2/d_{\text{SL}}v_{\text{gR}} \approx 12.6$ ns. The time of the longitudinal acoustic wave absorption in the bulk of the GaAs at 56 GHz frequency exceeds 2 ns.³⁴ In our experiments, the duration of the beatings in acoustically induced transient reflectivity signals (Figures 2b and 4a,c), resulting from the superposition of signals of comparable amplitudes due to bulk longitudinal acoustic wave and T waves, demonstrates that the lifetimes of the shear acoustic waves at ~ 50 GHz are, at least ~ 1 ns. Hence, it is expected that neither the diffraction nor the bulk absorption limits the gR wave lifetime in the experiments reported here.

This observation suggests that the gR wave lifetime could be further increased by either reducing the gR wave attenuation caused by surface roughness through improved surface quality (e.g., by depositing an oxide nanolayer to protect the surface from oxidation) or by minimizing gR wave energy emission to bulk modes through the design of an optimized SL structure and composition.

In the second sample, there is no apparent monitoring of L wave, which could be attributed to the reduced contrast in acoustic properties between the constituent layers of Al_{0.2}Ga_{0.8}As/Al_{0.4}Ga_{0.6}As SLs in the second sample in comparison to the GaAs/AlAs SL of the first sample. Alternatively, other factors related to sample fabrications, currently not fully understood, might contribute to this observation.

In summary, the transient reflectivity measurements from lateral scanning on the surfaces of both samples can be employed to unveil defects and the nanostructure geometry (including the interfaces of the SL with the surrounding materials) on micrometer scale through the evaluation of acoustic surface vibrations and bulk acoustic eigenmodes. Simultaneously, the monitoring of the gR wave on both samples strengthens the expectations that, in the near future, dedicated studies and optimized designs of the SL-based SAW nanotransducers will enhance the characteristics of the reported gR waves.

It is important to highlight that the signals from monitored T waves are notably prevalent in all our experiments. The following discussion clarifies why this observation has been somewhat unexpected. All forms of bulk acoustic waves, including quasi-longitudinal and quasi-transverse, can be detected using laser-induced gratings in transparent or weakly absorbing materials.^{35,36} The detection of L waves was previously reported in multiple experiments utilizing visible^{11,36} and UV laser-induced gratings,¹⁹ as well as deposited metallic gratings.^{37,38} Concomitantly, these gratings modulate (structure) the near-surface properties of the sample and modulate (ripple) the surface profile. However, there are relatively few reports³⁸ on T waves detection through laser-induced gratings in opaque materials. Additionally, we are not aware of any demonstrations of T wave generation and detection assisted by deposited metallic gratings.

A potential explanation for the absence of T waves in experiments with elastically isotropic gratings on an elastically isotropic substrate was previously provided.³⁹ In such elastically isotropic media, the most common laser-induced stresses, i.e., thermoelastic stresses, typically do not generate shear (transverse) acoustic waves within the bulk of the sample.³⁸ Theoretically, only the transverse mode that is mode-converted from the longitudinal mode, either incident at the surface or propagating along the surface, could contribute to shear surface displacement. Based on accumulated experimental^{37,40} and theoretical^{39,41} knowledge, it is anticipated that the structures in which either the substrate, the grating, or both exhibit elastic anisotropy, are better suited for controlling T waves. In the absence of elastic anisotropy, gR and L waves are expected to significantly dominate the acoustic signals in transient reflectivity measurements. This rationale aligns with our experimental demonstrations on cleaved SL structures composed of elastically anisotropic constituents. In our experiments, we have successfully accessed both gR and T waves, which feature extremely short but equal spatial periodicity. This characteristic results in a significant separation of their frequencies, even when their propagation velocities are closely matched. This platform provides promising opportunities to generate and detect T waves, thus avoiding potential signal interference from the presence of the gR wave. For instance, in isotropic media, measuring the velocity of T waves provides information on the shear rigidity of the material, a property entirely absent in L waves and mixed with information on the longitudinal modulus in the gR wave.^{14,42} Unlike L waves, T waves preferentially couple with rotational eigenmodes in materials with complex elasticity.^{43,44} In a nonexhaustive list of other advantageous applications of T waves, one can find the determination of residual stress,⁴⁵ inspection of material cracks,^{46,47} and evaluation of the dynamics of structural phase transitions.³⁶

CONCLUSIONS

We have successfully showcased the all-optical monitoring of the acoustic vibrations on the samples with periodically structured surface, prepared by cleavage of the SLs along their growth direction. In these structures the periodicity of the material parameters at cleaved mechanically free surface is due to their periodicity in the bulk. These samples, composed of nanometer pitch normally cleaved Al_xGa_{1-x}As/Al_yGa_{1-y}As SLs, were examined in pump-probe experiments utilizing visible (blue) pump and near-infrared probe laser beams from an ultrafast laser. These semiconductor SLs featured different

$\text{Al}_x\text{Ga}_{1-x}\text{As}$ constituent layers and a period of 71 nm. We observed and studied folded acoustic phonons, including gR, T, and L waves, within the frequency range of 40–70 GHz.

In this tested platform for studying surface acoustic motion at GHz frequencies, T waves dominate over gR waves and L waves. This dominance is tentatively attributed to the elastic anisotropy of the SL. It is worth noting that this may be related to the specific orientation of the SL layering relative to the nanostructure surface, which appears to favor the excitation of T waves by the gradients of the photoinduced stresses. However, it is essential to emphasize that this hypothesis would require further theoretical development, which is beyond the scope of our current presentation, primarily focused on experimental results.

Our platform provides opportunity to monitor T waves and gR waves independently due to the well-separated frequencies by tens of GHz in the nanotransducer. Our proof-of-concept experiments revealed the importance of phenomena such as the oxidation of the freshly cleaved surface, the surface roughness, and the non-negligible smallness of the elastic contrast between the layers on the efficiency of SAWs monitoring by laser on the suggested platform. By optimizing these factors along with diminishing the SL period, our platform holds practical opportunities to break the current limitation of SAW frequency, extending it to sub-THz range.

Our experimental findings provide a viable solution for monitoring surface acoustic vibrations with GHz frequencies. This approach serves as a valuable alternative and supplement to established techniques involving metal grating and EUV light grating methods. Unfortunately, our initial trial experiments on the same nanostructured samples, aimed at demonstrating the propagation of the gR wave packets between two spatially separated points on the sample surface by focusing the pump and probe laser beams on these points, expectedly failed. The limited length of gR wave propagation on our SLs, estimated to be approximately $l_{\text{gR}} \approx 1.9 \mu\text{m}$ based on the estimated gR wave lifetime and velocity, is comparable to the diameter of the laser beams ($\approx 1.64 \mu\text{m}$). These laser beams dictate the lengths of the monitored gR wave packet. Consequently, the pump and probe laser beams essentially overlap, even when the centers of the pump and probe laser beams are separated by the gR wave propagation distance. Moreover, the gR wave propagation time between the focal points is similar to its duration. In simpler terms, the signal increase resulting from the forward movement of the gR wave packet, generated in the pump focus region, toward the detection area controlled by the spatially shifted probe focus, is significantly suppressed or saturated due to the attenuation of gR wave packet happening on the same time scale. This led to gR wave signals falling below the noise level.

Several potential approaches exist for future monitoring of gR wave packets. First, it is desirable to increase the propagation lengths of gR waves. This can be accomplished by reducing surface roughness and preventing surface oxidation. To mitigate oxidation, a protective oxide nanolayer can be applied to the surface immediately after cleaving the SL, or the SLs can be grown from oxide material components. Second, shortening the length/duration of the monitored gR wave packets is desirable. This can be achieved by employing stronger laser focusing or by reducing the thickness of the SL to be smaller than the diameter of the laser foci.

Furthermore, it is crucial to combine these approaches with the optimal selection of materials for the SL layers. Material

optimization entails enhancing optoacoustic and acousto-optic transformation efficiencies at specific wavelengths of the pump and probe lasers. By improving these efficiencies, the amplitude of the signal resulting from coherent gR waves would increase, potentially elevating gR wave amplitudes above the noise level at micrometer propagation distances.

Sub-THz SAWs are potentially promising for future applications in science and technology, such as the next generation of ICT devices well beyond the 5G standard (600 MHz to 6 GHz). The recent demonstration of picosecond acoustics based on miniaturized lasers¹⁶ represents a significant step forward in applying laser-monitored SAWs to future ICT. A detailed understanding of the propagation of such SAWs on atomically flat surfaces and across material junctions is a prerequisite for accessing the fundamental concepts of thermal load management. With the diminishing periodicity of the SL, the platform of the cleaved SLs presented herein also holds considerable potential for revealing and exploring strong acousto-optic and opto-acoustic interactions due to the simultaneous confinement of acoustic and electromagnetic modes.

METHODS

A. Sample Preparation and Characterization by X-ray Diffraction and AFM. The SL samples were grown using solid-source molecular beam epitaxy (MBE) with a Veeco GenXplor system. The $\text{Al}_x\text{Ga}_{1-x}\text{As}$ alloy was achieved through a digital alloy growth technique, where the composition is determined by the layer thicknesses of GaAs and AlAs. The samples were grown under typical conditions for GaAs and AlAs, maintaining an As-rich environment at 580 °C. The growth rates were approximately 1 ML/s for both GaAs and AlAs. High-resolution XRD scans on the (004) plane were conducted using a Bruker D8 system. AFM measurements were performed with a 5500 AFM from Agilent in intermittent contact mode in air (cantilever stiffness was 40 N/m). Image processing utilized Gwyddion freeware.

B. Structure of the Generalized Rayleigh SAWs in Cleaved SLs. For the physical interpretation of the demonstrated all-optical monitoring of the Rayleigh-type SAW (R) wave on the SL stratified normal to the surface, it is important to emphasize the key differences in the mode structure of this gR wave compared to the Rayleigh SAW (RSAW) on the surface of a homogeneous half-space. As explained by the Bloch–Floquet theorem,⁴⁸ there is an infinite number of the bulk longitudinal and transverse wave eigenmodes in the SL presented in Figure 2c. This is attributed to the periodicity of SL parameters, characterized by the spatial period d_{SL} or by the SL (Floquet) wavenumber $q_{\text{SL}} = 2\pi/d_{\text{SL}}$ along the x_1 axis (the direction of SL layering).

The m th order bulk eigenmodes can be viewed as the diffraction orders of the bulk modes with frequency ω and the wave vector \vec{k} (with $k_2 = 0$ for the waves polarized in the sagittal plane (x_1x_3)), which differ by the projections of k_1 ($k_1 + mq_{\text{SL}}, m = 0, \pm 1, \pm 2, \dots$) on the x_1 -axis. Crucially, the displacement components with different m are parametrically coupled due to the periodicity of the acoustical properties in the SL. Consequently, each eigenmodes, numbered as the m th mode, contains components with all allowed $m = 0, \pm 1, \pm 2, \dots$, including, in general, $m = 0$, although with different amplitudes.

The gR wave results from the superposition of the bulk modes, evanescent in the depth direction x_3 (i.e., with k_3 describing amplitude decay with depth) and satisfying periodic stress-free boundary condition on $x_3 = 0$ at a particular gR wave eigenfrequency, ω_{gR} . It contains displacement components with all $k_1 + mq_{\text{SL}}, m = 0, \pm 1, \pm 2, \dots$ (see Supporting Information, S1, for details). Similar to the dispersion relations for bulk acoustic waves, the gR wave dispersion relation can be folded in the Brillouin zone with the acoustic phonon branches, starting from $\omega = 0$, and the optical phonons branches.^{28,49} The important difference of the gR wave from RSAW is that the former

contains, in the zone-center $k_1 = 0$, laterally nonmodulated displacement and strain components at the frequencies of optical-type SAWs.

C. Photogeneration of the Coherent Acoustic Eigenmodes in Cleaved SLs. In our experiments, the phonons in the close vicinity of the Brillouin zone center, i.e., with $k_1 \ll q_{\text{SL}} \equiv 2\pi/d_{\text{SL}}$, play the dominant role, as evident from the fact that the radii of pump and probe laser beams foci on the SL surface, $a_{\text{pump}} \approx a_{\text{probe}} \approx a$, significantly exceed the SL period d_{SL} . The k spectrum of the photogenerated SAWs is controlled by the lateral distribution of the stresses, photoinduced by the pump laser pulses (see Supporting Information, S1, for the details). In our experiments, the lateral modulation of the photoinduced stresses on the nanometer spatial scale is mostly due to the difference in the optical properties of the two layers.

In the infinite SL, the stresses photoinduced by laterally homogeneous pump laser radiation will have the periodicity of the SL and exhibit the Bloch–Floquet property. Thus, the folded k_1 spectrum of the photoinduced stresses would contain only zone center components, $k_1 = 0$. Focusing the pump laser radiation in a spot with radius a localizes laterally the photoinduced stresses on the scale $a \gg d_{\text{SL}}$, even in the case of a diffraction-limited focusing, because of the suboptical periodicity of the SL, i.e., $d_{\text{SL}}/\lambda \ll 1$. Therefore, the related broadening of the k_1 spectrum components is much narrower than the width of the Brillouin zone π/d_{SL} and the photogenerated gR wave spectrum is strongly localized near the Brillouin zone center.

The condition $a \gg d_{\text{SL}}$ also leads to the expectations that symmetric motions of individual SL layers are photoexcited with larger amplitudes than antisymmetric ones. Here, we denote symmetric modes as modes that exhibits an odd distribution of the horizontal mechanical displacement, u_1 , and an even distribution of vertical mechanical displacement, u_3 , relative to the central plane of the individual layer (see Supporting Information, S1, for the details).

For the experimental platform of a semi-infinite SL stratified normal to the surface, it is crucial that the zone-center surface confined modes contain laterally homogeneous components in their structure. This implies that gR modes can be excited by a laterally homogeneous (averaged over the SL period) part of the distributed photoinduced stresses or, in principle, even by laterally nonmodulated stresses in the hypothetical case of the absence of optical but existing acoustical contrast between the SL composing layers.

Under the condition of weak acoustical contrast, $\Delta\rho/\langle\rho\rangle \sim \Delta C_{ij}/\langle C_{ij}\rangle \sim \mu \ll 1$, which is sufficiently well satisfied in our experimental samples, the amplitude ratio of the nonmodulated to modulated zone-center gR wave components scales with $\sim\mu$, the frequency of the lowest zone center optical-type gR wave, ω_{gR} , deviates from the respective frequency ω_{gR} of RSAW with the wave vector $k_1 = 2\pi/d_{\text{SL}}$ in the medium of the period-averaged parameters, $\text{Re}(\omega_{\text{gR}} - \omega_{\text{R}})/\omega_{\text{R}} \sim \mu^2$, and it acquires an imaginary part $\text{Im}(\omega_{\text{gR}})/\omega_{\text{R}} \sim \mu^2$. Thus, the zone center gR waves are actually pseudo-SAWs.^{5b,51}

D. Photodetection of the Coherent Acoustic Eigenmodes in Cleaved SLs. The laterally homogeneous components of the high frequency acoustic eigenmodes in cleaved SLs can be detected by probe laser radiation, as established in picosecond laser ultrasonics of depth-stratified samples/structures.⁵² The theoretical analysis of the detection paths of gR wave, when it is propagating in the SL (identical to the one where it was photogenerated), reveals that the laterally modulated components of the gR wave can also be efficiently detected due to the lateral periodicity in the SL of the optical permittivity ϵ and/or the photoelastic parameter p (see Supporting Information, S2, for the details).

The essence of the acoustic wave detection in the ultrafast pump–probe optical experiments (via measurements of the transient reflectivity at normal incidence of probe laser light) is the heterodyning of the weak acoustically scattered probe light by the strong probe light reflected from the surface of the SL.⁵³ Only the probe light reflected in the $m = 0$ diffraction order reaches the photodetector because the light reflected in the other diffraction orders is evanescent due to suboptical periodicity of the considered

cleaved SLs. Consequently, only the probe light scattered by the acoustical wave in the zeroth diffraction order is detectable.

An additional consequence of the suboptical periodicity of the SL is that each diffraction of light by the modulated components of the SL parameters acquires a multiplier $(d_{\text{SL}}/\lambda)^2 \ll 1$ in the amplitude of the diffracted light. Because of this, the nonevanescing probe light that can propagate in the direction of the photodetector (in the zeroth diffraction order) after exhibiting several consecutive diffractions (in reflection and/or scattering) is negligibly small in amplitude compared to the nondiffracted probe light.

Only the scattering of the nondiffracted probe light by the acoustically induced modulation of the period-averaged optical permittivity $\langle\epsilon\rangle$ of the SL should be considered. However, this laterally homogeneous modulation is caused not only by the modulation of the averaged permittivity by the laterally nonmodulated gR wave component (first path) but also by the demodulation of the laterally modulated components of the gR wave when it interacts with SL parameters, exhibiting the same periodicity as the gR wave (second path). From the viewpoint of formal mathematics, the second path is due to the presence of the constant/infinite-period term in the square of the sine/cosine functions. In particular, the second path of the possible detection can be due to $\epsilon^{(1)} - \epsilon^{(2)} \neq 0$ and/or $(\epsilon^{(1)})^2 p^{(1)} - (\epsilon^{(2)})^2 p^{(2)} \neq 0$, i.e., due to optical or/and acousto-optical contrast between the SL layers (see Supporting Information, S2).

Note that, in the case $\epsilon^{(1)} - \epsilon^{(2)} \neq 0$, the second detection path can be due to the difference in the individual layer thickness variations induced by horizontal displacements components of the gR wave even in the case of the negligible photoelasticity of both layers ($p = 0$). The theory indicates that either the first or the second detection path could dominate depending on the relative strengths of the acoustical (density ρ , elastic moduli C_{ij}) or optical/acousto-optical (permittivity, photoelastic moduli) contrasts between the SL layers. The first path progressively disappears with diminishing acoustic contrast because of the disappearance of the laterally unmodulated component of gR wave. However, it could still be the dominant path in the hypothetical case of the absence of optical and acousto-optical contrasts (see Supporting Information, S2, for the details).

Overall, the inevitable diminishing of the detected gR wave signals with the diminishing of the suboptical SL pitch ($\sim d_{\text{SL}}/\lambda$, see Supporting Information, S2) is not the direct consequence of the fall in light diffraction efficiency due to nanometer scale periodicity but is caused by the diminishing of the acousto-optic scattering volume proportionally to the penetration depth of the gR wave, $\sim d_{\text{SL}}$.

E. Ultrafast Pump–Probe Laser Experiments. The acoustic vibrations are monitored through ultrafast pump–probe experiments employing a femtosecond laser. A Ti:sapphire laser (Spectra-Physics) with a central wavelength of 810 nm, a pulse width of ~ 100 fs, and a pulse repetition rate of ~ 80 MHz is utilized. The laser beam at the fundamental wavelength probes the sample, while the laser beam at the second harmonic, generated in a BBO crystal, is employed to pump/excite the sample. A translation stage inserted in the pump path induces the pump–probe delay, with a maximum range of ~ 8 ns.

The attenuated pump and probe laser beams are collinearly focused by an objective (100 \times , NA of 0.55) on the same surface of the sample. The reflected probe light is detected by a large-area 150 kHz bandwidth photoreceiver (NewFocus, model 2031), whose output is connected to a lock-in amplifier for synchronous detection at the 150 kHz modulation frequency of the pump intensity. This allows for low-noise signal acquisition, transmitted to an analogue-to-digital convertor for data collection. To test different lateral positions on the sample surface, the sample is displaced relative to laser foci by a translation stage.

F. Signal Processing Methods.

- (a) *Background Deletion.* The time-dependent reflectivity change undergoes numerical processing to reveal small-amplitude acoustic oscillations. These oscillations are extracted by subtracting the nonoscillating background from the raw signal. The background is obtained using a moving average method with a Gaussian window duration of approximately 100 ps.

Removing the background does not introduce any new frequency appearances or alterations; instead, it suppresses undesired relatively low frequency components or environmental/mechanical/thermal noises.

- (b) *Fourier Transform.* The spectra are obtained by applying fast Fourier transform (FFT) to the time-domain acoustic signals. A Hanning window is multiplied over the signal of interest for FFT.
- (c) *Short-Time FFT.* To observe time-dependent changes in spectra amplitude (Figure 2d) and for the second sample (Figure 5d), a short-time FFT procedure is used. During the procedure, the parameters include Gaussian window of 400 ps duration, a frequency resolution for frequency axis of 0.1 GHz, and a hop time of 10 ps.

G. Finite Element Model (Dispersion Relation and Acoustic Eigenmodes). The dispersion curves of surface acoustic waves (SAWs) propagating at the free surface of assumed infinitely cleaved superlattices are computed using finite element method (FEM) with eigenfrequency analysis in COMSOL Multiphysics.

- (a) *Structure, Material, and Boundaries.* A unit of the superlattice, consisting of alternating two layers with a period of d_{SL} is constructed (see Supporting Information, S1, for details on the structure). The height of the superlattice along the x_3 direction is set to $20d_{\text{SL}}$. The [100] crystallographic orientation of constitutive materials is aligned with the x_1 axis (SL growth direction) in the calculation. Because the displacement component normal to the x_1x_3 plane equals zero, the model is treated as a 2D problem. The two layers are considered as linear elastic cubic materials based on $\text{Al}_x\text{Ga}_{1-x}\text{As}$. Floquet periodic boundary conditions are applied to the left and right sides of the unit cell along the x_1 direction. The top surface is assumed to be a stress-free boundary. A perfectly matched layer (PML) is placed at the bottom of the unit cell to simulate an infinite half-space. The bottom surface of the unit cell is set as a fixed boundary to limit the acoustic eigenmodes localized at that bottom surface. The PML length is set as one period of the SL.
- (b) *Calculation.* The solid mechanics interface of the structural mechanics module of the COMSOL Multiphysics is used to solve an eigenfrequency problem based on the elastic Helmholtz equation. The eigenfrequencies are searched through a parametric sweep over the first Brillouin zone $k_1 \in [0, \pi/d_{\text{SL}}]$ with a step of $\pi/d_{\text{SL}}/100$. The eigenvalue solver is MUMPS (multifrontal massively parallel sparse direct solver), set to look for 1000 eigenfrequencies to find all the relevant eigenvalues. The eigenvectors for each solution correspond to the mode shape, including the horizontal displacement u_1 (along x_1 -axis) and the vertical displacement u_3 (along x_3 -axis). The computation time for these settings was 6 h 33 min on a computer (Intel core i9-9980HK CPU@2.4 GHz).
- (c) *Mode Sorting.* First, solutions with a large imaginary part of its eigenfrequency are excluded. Second, the mode shape (displacement field or energy spatial distribution) of the remaining solutions is used to distinguish the gR wave (confined close to the surface, see Figure 3a), T wave (with dominant vertical displacement, see Figure 3b) and L wave (with dominant horizontal displacement, see Figure 3b) modes. At last, for validation, the obtained mode branches are compared to their expected phase velocities.

H. Brillouin Light Scattering in Cleaved SLs. The efficient backward scattering of the probe light in the zeroth order of diffraction, the only nonvanishing light field component in the deeply suboptical SL, is governed by the momentum conservation conditions $k_1 = q_1 = 0$ and $k_3 = 2q_3$, where k_i and q_i denote the components of the acoustic and probe light wave vectors, respectively. The normal components k_3 of the coherent acoustic waves in the different diffraction orders m are given by

$$k_{3,\text{QTA,QLA}} = \sqrt{k_{\text{QTA,QLA}}^2 - (2\pi m/d_{\text{SL}})^2}$$

where $k_{\text{QTA,QLA}} = \omega/v_{\text{QTA,QLA}}$ are the wave vectors of the quasi-transversal (QTA) and quasi-longitudinal (QLA) acoustic waves propagating along the directions of the respective diffraction orders in the SL, d_{SL} is the SL period and $m = 0, \pm 1, \pm 2, \dots$. Therefore, the velocities $v_{\text{QTA,QLA}}$ of the QTA and QLA waves in the above formula should be evaluated along the directions defined by the following angles $\gamma \equiv \gamma(d_{\text{SL}}, m) = \tan^{-1}[(2\pi m/d_{\text{SL}})/k_{3,\text{QTA,QLA}}] = \tan^{-1}[(2\pi m/d_{\text{SL}})/(2q_3)]$ relative to the x_3 axis. Thus, the knowledge of the probe light wave vector and the slowness curves (anisotropy) of the acoustic modes in the SL provides an opportunity to estimate the Brillouin frequencies.

In our estimates, as described in Supporting Information, S1, and based on the weak elastic contrast between the layers, we used the dependences of the acoustic velocities on the propagation direction/angle provided by the slowness curves of the GaAs⁴² and averaged optical refractive index $\langle n \rangle$. Two of the spectral peaks in the lower part of Figure 2c can be tentatively attributed to Brillouin scattering of probe by QLA waves in the orders $m = 0$ and $m = 1$, respectively. All these waves are nonvanishing. Note that symmetry considerations prevent the generation of the QTA waves with the order $m = 0$ in our experimental configuration.⁴² It is also worth noting that the SL is optically birefringent,⁵⁴ and thus, potentially each of the Brillouin peaks could be composed of up to three neighboring spectral components, corresponding to different combinations of ordinary and extraordinary probe light propagating from and toward the SL surface.⁵⁵ We have experimentally verified that the position of the most intense Brillouin peak around 45.7 GHz (Figure 2c) depends on the polarization of the probe light. However, the splitting of the peak is not resolved in our experiments because of weak birefringence, which is caused only by structuring, while the materials of the SL layers are optically isotropic.

ASSOCIATED CONTENT

Supporting Information

The Supporting Information is available free of charge at <https://pubs.acs.org/doi/10.1021/acsnano.3c07576>.

Structure of generalized Rayleigh-type surface acoustic wave on a superlattice stratified normal to its surface; Optical detection of generalized Rayleigh-type surface acoustic wave on a superlattice stratified normal to its surface (PDF)

AUTHOR INFORMATION

Corresponding Author

Vitaliy E. Gusev – *Laboratoire d'Acoustique de l'Université du Mans (LAUM), UMR 6613, Institut d'Acoustique – Graduate School (IA-GS), CNRS, Le Mans Université, 72085 Le Mans, France;* orcid.org/0000-0002-2394-7892; Email: vitali.goussev@univ-lemans.fr

Authors

Changxiu Li – *Laboratoire d'Acoustique de l'Université du Mans (LAUM), UMR 6613, Institut d'Acoustique – Graduate School (IA-GS), CNRS, Le Mans Université, 72085 Le Mans, France;* orcid.org/0000-0003-2875-9441

Nikolay Chigarev – *Laboratoire d'Acoustique de l'Université du Mans (LAUM), UMR 6613, Institut d'Acoustique – Graduate School (IA-GS), CNRS, Le Mans Université, 72085 Le Mans, France;* orcid.org/0000-0002-2902-9363

Théo Thérard – *Laboratoire d'Acoustique de l'Université du Mans (LAUM), UMR 6613, Institut d'Acoustique – Graduate School (IA-GS), CNRS, Le Mans Université, 72085 Le Mans, France;* orcid.org/0000-0001-5930-4306

Kedong Zhang – College of Engineering and Applied Sciences, Nanjing University, 210093 Nanjing, China

Nicolas Delorme – Institut des Molécules et Matériaux du Mans (IMMM), UMR 6283 CNRS, Le Mans Université, 72085 Le Mans, France; orcid.org/0000-0003-4195-2000

Vincent Tournat – Laboratoire d'Acoustique de l'Université du Mans (LAUM), UMR 6613, Institut d'Acoustique – Graduate School (IA-GS), CNRS, Le Mans Université, 72085 Le Mans, France; orcid.org/0000-0003-4497-5742

Samuel Raetz – Laboratoire d'Acoustique de l'Université du Mans (LAUM), UMR 6613, Institut d'Acoustique – Graduate School (IA-GS), CNRS, Le Mans Université, 72085 Le Mans, France; orcid.org/0000-0003-3683-8764

Hong Lu – College of Engineering and Applied Sciences, Nanjing University, 210093 Nanjing, China; orcid.org/0000-0002-8340-2739

Complete contact information is available at: <https://pubs.acs.org/10.1021/acsnano.3c07576>

Author Contributions

C.L. conducted the experiments, executed the simulations and input corresponding sections for the manuscript. N.C. conducted the first experimental tests and helped with the experiments. T.T. participated the first trial experiments. V.T. helped with the initial simulations. N.D. conducted the AFM characterization. H.L. and K.Z. prepared and characterized the samples by XRD. S.R. assisted with signal processing, improved the manuscript. V.G. and H.L. designed the samples. V.G. designed the methodology, wrote the first manuscript and supervised the project. All authors reviewed the manuscript.

Notes

The authors declare no competing financial interest.

ACKNOWLEDGMENTS

This research is supported by the postdoctoral fellowships of the Institut d'Acoustique–Graduate School (IA-GS) of Le Mans Université and of European Commission's Horizon 2020 research and innovation programme under the Marie Skłodowska-Curie grant agreement no. 101025424 for C. Li.

ABBREVIATIONS

RSAW, Rayleigh surface acoustic wave; SL, superlattice; SAW, surface acoustic wave; OA, optoacoustic; AO, acousto-optic; OAOT, opto-acousto-optic transducer; EUV, extreme ultraviolet; NIR, near-infrared; MBE, molecular beam epitaxy; XRD, X-ray diffraction; AFM, atomic force microscopy; gR, generalized Rayleigh surface acoustic wave; T, skimming surface transverse acoustic wave; L, skimming surface longitudinal acoustic wave; QLA, quasi-longitudinal acoustic; QTA, quasi-transversal acoustic.

REFERENCES

- (1) White, R.; Voltmer, F. Direct Piezoelectric Coupling to Surface Elastic Waves. *Appl. Phys. Lett.* **1965**, *7*, 314–316.
- (2) Lee, R.; White, R. M. Excitation of Surface Elastic Waves by Transient Surface Heating. *Appl. Phys. Lett.* **1968**, *12*, 12–14.
- (3) Morgan, D. *Surface Acoustic Wave Filters: With Applications to Electronic Communications and Signal Processing*; Elsevier Science: Amsterdam, 2010.
- (4) Hess, P. Laser Diagnostics of Mechanical and Elastic Properties of Silicon and Carbon Films. *Appl. Surf. Sci.* **1996**, *106*, 429–437.
- (5) de Lima, M. M., Jr.; Santos, P. V. Modulation of Photonic Structures by Surface Acoustic Waves. *Rep. Prog. Phys.* **2005**, *68*, 1639–1701.
- (6) Fuhrmann, D. A.; Thon, S. M.; Kim, H.; Bouwmeester, D.; Petroff, P. M.; Wixforth, A.; Krenner, H. J. Dynamic Modulation of Photonic Crystal Nanocavities Using Gigahertz Acoustic Phonons. *Nat. Photonics* **2011**, *5*, 605–609.
- (7) Bahl, G.; Zehnpfennig, J.; Tomes, M.; Carmon, T. Stimulated Optomechanical Excitation of Surface Acoustic Waves in a Microdevice. *Nat. Commun.* **2011**, *2*, 403.
- (8) Rocke, C.; Zimmermann, S.; Wixforth, A.; Kotthaus, J. P.; Böhm, G.; Weimann, G. Acoustically Driven Storage of Light in a Quantum Well. *Phys. Rev. Lett.* **1997**, *78*, 4099.
- (9) Naber, W.; Fujisawa, T.; Liu, H.; van der Wiel, W. G. Surface Acoustic-Wave-Induced Transport in a Double Quantum Dot. *Phys. Rev. Lett.* **2006**, *96*, No. 136807.
- (10) Couto, O. D. D.; Iikawa, F.; Rudolph, J.; Hey, R.; Santos, P. V. Anisotropic Spin Transport in (110) GaAs Quantum Wells. *Phys. Rev. Lett.* **2007**, *98*, No. 036603.
- (11) Janušonis, J.; Jansma, T.; Chang, C.; Liu, Q.; Gatilova, A.; Lomonosov, A.; Shalagatskiy, V.; Pezeril, T.; Temnov, V.; Tobey, R. Transient Grating Spectroscopy in Magnetic Thin Films: Simultaneous Detection of Elastic and Magnetic Dynamics. *Sci. Rep.* **2016**, *6*, No. 29143.
- (12) Kukushkin, I. V.; Smet, J. H.; Scarola, V. W.; Umansky, V.; von Klitzing, K. Dispersion of Excitations of Fractional Quantum Hall States. *Science* **2009**, *324*, 1044.
- (13) Schubert, M.; Grossmann, M.; Ristow, O.; Hettich, M.; Bruchhausen, A.; Barretto, E. C. S.; Scheer, E.; Gusev, V.; Dekorsy, T. Spatial-Temporally Resolved High-Frequency Surface Acoustic Waves on Silicon Investigated by Femtosecond Spectroscopy. *Appl. Phys. Lett.* **2012**, *101*, No. 013108.
- (14) Gusev, V. E.; Karabutov, A. A. *Laser Optoacoustics*; Nauka: Moscow, 1991; AIP: New York, 1993.
- (15) Kasinski, J. J.; Gomez-Jahn, L.; Leong, K.; Gracewski, S. M.; Dwayne Miller, R. J. Optical Generation of Coherent Surface Acoustics: an Optically Based Probe of Surface Structure and Dynamics. *Opt. Lett.* **1988**, *13*, 710–712.
- (16) Harata, A.; Nishimura, H.; Sawada, T. Laser-Induced Surface Acoustic Waves and Photothermal Surface Gratings Generated by Crossing Two Pulsed Laser Beams. *Appl. Phys. Lett.* **1990**, *57*, 132–134.
- (17) Rogers, J. A.; Maznev, A. A.; Banet, M. J.; Nelson, K. A. Optical Generation and Characterization of Acoustic Waves in Thin Films: Fundamental and Applications. *Annu. Rev. Mater. Sci.* **2000**, *30*, 117–157.
- (18) Maznev, A. A.; Mincigrucchi, R.; Bencivenga, F.; Unikandanunni, V.; Capotondi, F.; Chen, G.; Ding, Z.; Duncan, R. A.; Foglia, L.; Izzo, M. G.; et al. Generation and Detection of 50 GHz Surface Acoustic Waves by Extreme Ultraviolet Pulses. *Appl. Phys. Lett.* **2021**, *119*, No. 044102.
- (19) Bencivenga, F.; Mincigrucchi, R.; Capotondi, F.; Foglia, L.; Naumenko, D.; Maznev, A. A.; Pedersoli, E.; Simoncig, A.; Caporaletti, F.; Chiloyan, V.; et al. Nanoscale Transient Gratings Excited and Probed by Extreme Ultraviolet Femtosecond Pulses. *Sci. Adv.* **2019**, *5*, No. eaaw5805.
- (20) Bonello, B.; Ajinou, A.; Richard, V.; Djemia, P.; Cherif, S. M. Surface Acoustic Waves in the GHz Range Generated by Periodically Patterned Metallic Stripes Illuminated by an Ultrashort Laser Pulse. *J. Acoust. Soc. Am.* **2001**, *110*, 1943–1949.
- (21) Hurley, D. H.; Telschow, K. L. Picosecond Surface Acoustic Waves Using a Suboptical Wavelength Absorption Grating. *Phys. Rev. B* **2002**, *66*, No. 153301.
- (22) Li, Q.; Hoogeboom-Pot, K.; Nardi, D.; Murnane, M. M.; Kapteyn, H. C.; Siemens, M. E.; Anderson, E. H.; Hellwig, O.; Dobisz, E.; Gurney, B.; et al. Generation and Control of Ultrashort-

Wavelength Two-Dimensional Surface Acoustic Waves at Nanoscale Interfaces. *Phys. Rev. B* **2012**, *85*, No. 195431.

(23) Wirtz, T.; De Castro, O.; Audinot, J.-N.; Philipp, P. Imaging and Analytics on the Helium Ion Microscope. *Annu. Rev. Anal. Chem.* **2019**, *12*, 523–543.

(24) Li, W.-D.; Wu, W.; Stanley Williams, R. Combined Helium Ion Beam and Nanoimprint Lithography Attains 4 nm Half-Pitch Dense Patterns. *J. Vac. Sci. Technol. B* **2012**, *30*, No. 06F304.

(25) Manfrinato, V. R.; Camino, F. E.; Stein, A.; Zhang, L.; Lu, M.; Stach, E. A.; Black, C. T. Patterning Si at the 1 nm Length Scale with Aberration-Corrected Electron-Beam Lithography: Tuning of Plasmonic Properties by Design. *Adv. Funct. Mater.* **2019**, *29*, No. 1903429.

(26) Huynh, A.; Perrin, B.; Lemaître, A. Semiconductor Superlattices: a Tool for Terahertz Acoustics. *Ultrasonics* **2015**, *56*, 66–79.

(27) Maznev, A. A.; Hung, T.-C.; Yao, Y.-T.; Chou, T.-H.; Gandhi, J. S.; Lindsay, L.; Shin, H. D.; Stokes, D. W.; Forrest, R. L.; Bensaoula, A.; et al. Propagation of THz Acoustic Wave Packets in GaN at Room Temperature. *Appl. Phys. Lett.* **2018**, *112*, No. 061903.

(28) Djafari-Rouhani, B.; Maradudin, A. A.; Wallis, R. F. Rayleigh Waves on a Superlattice Stratified Normal to the Surface. *Phys. Rev. B* **1984**, *29*, 6454.

(29) Gusev, V. E. Laser Generation of High-Frequency Rayleigh Surface Acoustic Waves in Normally Cut Superlattices. *Opt. Acoust. Rev.* **1990**, *1*, 238–249.

(30) Gusev, V. E. On the Possibility of Rayleigh-Type Surface Acoustic Waves Excitation at Frequencies up to 10–100 GHz by Laser Action on a Normally Cut Superlattice. In *Photoacoustic and Photothermal Phenomena III*; Bičanić, D., Ed; Springer: Berlin, 1992; pp 323–325.

(31) Choquette, K. D.; Geib, K. M.; Ashby, C. I. H.; Twisten, R. D.; Blum, O.; Hou, H. Q.; Follstaedt, D. M.; Hammons, B. E.; Mathes, D.; Hull, R. Advances in Selective Wet Oxidation of AlGaAs Alloys. *IEEE J. Sel. Top. Quantum Electron.* **1997**, *3*, 916–926.

(32) Ruello, P.; Gusev, V. E. Physical Mechanisms of Coherent Acoustic Phonons Generation by Ultrafast Laser Action. *Ultrasonics* **2015**, *56*, 21–35.

(33) Brekhovskikh, L. M. Propagation of Surface Rayleigh Waves along the Uneven Boundary of an Elastic Body. *Sov. Phys. Acoust.* **1960**, *5*, 288–295.

(34) Chen, W.; Maris, H. L.; Wasilewski, Z. R.; Tamura, S.-I. Attenuation and Velocity of 56 GHz Longitudinal Phonons in Gallium Arsenide from 50 to 300 K. *Philos. Mag. B* **1994**, *70*, 687–698.

(35) Fayer, M. Picosecond Holographic Grating Generation of Ultrasonic Waves. *IEEE J. Quantum Electron.* **1986**, *22*, 1437–1452.

(36) Robinson, M. M.; Yan, Y. X.; Gamble Jr, E. B.; Williams, L. R.; Meth, J. S.; Nelson, K. A. Picosecond Impulsive Stimulated Brillouin Scattering: Optical Excitation of Coherent Transverse Acoustic Waves and Application to Time-Domain Investigations of Structural Phase Transitions. *Chem. Phys. Lett.* **1984**, *112*, 491–496.

(37) Stoklasová, P.; Grabec, T.; Zoubková, K.; Sedláč, P.; Krátký, S.; Seiner, H. Laser-Ultrasonic Characterization of Strongly Anisotropic Materials by Transient Grating Spectroscopy. *Exp. Mech.* **2021**, *61*, 663–676.

(38) Matsuda, O.; Pezeril, T.; Chaban, I.; Fujita, K.; Gusev, V. Time-Domain Brillouin Scattering Assisted by Diffraction Gratings. *Phys. Rev. B* **2018**, *97*, No. 064301.

(39) Kolomenskii, A. A.; Maznev, A. A. Surface Responses in the Laser Irradiation of a Solid-Rayleigh-Waves and Precursors. *Sov. Phys. Acous.* **1990**, *36*, 463–469.

(40) Matsuda, O.; Tsutsui, K.; Vaudel, G.; Pezeril, T.; Fujita, K.; Gusev, V. Optical Generation and Detection of Gigahertz Shear Acoustic Waves in Solids Assisted by a Metallic Diffraction Grating. *Phys. Rev. B* **2020**, *101*, No. 224307.

(41) Maznev, A. A.; Every, A. G. Time-Domain Dynamic Surface Response of an Anisotropic Elastic Solid to an Impulsive Line Force. *Int. J. Eng. Sci.* **1997**, *35*, 321–327.

(42) Auld, B. A. *Acoustic Fields and Waves in Solids*; John Wiley & Sons: New York, 1973.

(43) Cabaret, J.; Béquin, P.; Theocharis, G.; Andreev, V.; Gusev, V. E.; Tournat, V. Nonlinear hysteretic torsional waves. *Phys. Rev. Lett.* **2015**, *115*, No. 054301.

(44) Lomonosov, A. M.; Yan, X.; Sheng, C.; Gusev, V. E.; Ni, C.; Shen, Z. Exceptional Elastic Anisotropy of Hybrid Organic-Inorganic Perovskite CH₃NH₃PbBr₃ Measured by Laser Ultrasonic Technique. *Phys. Status Solidi-R* **2016**, *10*, 606–612.

(45) Sathish, S.; Martin, R. W.; Moran, T. J. Local Surface Skimming Longitudinal Wave Velocity and Residual Stress Mapping. *J. Acoust. Soc. Am.* **2004**, *115*, 165–171.

(46) Ni, C. Y.; Chigarev, N.; Tournat, V.; Delorme, N.; Shen, Z. H.; Gusev, V. E. Probing of Laser-Induced Crack Modulation by Laser-Monitored Surface Waves and Surface Skimming Bulk Waves. *J. Acoust. Soc. Am.* **2012**, *131*, EL250–EL255.

(47) Chigarev, N.; Zinin, P.; Ming, L. C.; Amulele, G.; Bulou, A.; Gusev, V. Laser Generation and Detection of Longitudinal and Shear Acoustic Waves in a Diamond Anvil Cell. *Appl. Phys. Lett.* **2008**, *93*, No. 181905.

(48) Kittel, C. *Introduction to Solid State Physics*; John Wiley & Sons: Singapore, 1996.

(49) Colvard, C.; Gant, T. A.; Klein, M. V.; Merlin, R.; Fischer, R.; Morkoc, H.; Gossard, A. C. Folded Acoustic and Quantized Optic Phonons in (GaAl)As Superlattices. *Phys. Rev. B* **1985**, *31*, 2080–2091.

(50) Farnell, G. W.; Adler, E. L. Elastic Wave Propagation in Thin Layers. In *Physical Acoustics: Principles and Methods*; Mason, W. P., Thurston, R. N., Eds.; Academic Press: New York, 1972; Vol. 9; pp 35–127.

(51) da Cunha, M. P. Pseudo and High Velocity Pseudo SAWs. In *Advances in Surface Acoustic Wave Technology, Systems and Applications*; Ruppel, C. C. W., Fjeldly, T. A., Eds.; World Scientific: Singapore, 2001; Vol. 2; pp 203–243.

(52) Bartels, A.; Dekorsy, T.; Kurz, H.; Köhler, K. Coherent Zone-Folded Longitudinal Acoustic Phonons in Semiconductor Superlattices: Excitation and Detection. *Phys. Rev. Lett.* **1999**, *82*, 1044–1047.

(53) Thomsen, C.; Grahn, H. T.; Maris, H. J.; Tauc, J. Surface Generation and Detection of Phonons by Picosecond Light Pulses. *Phys. Rev. B* **1986**, *34*, 4129.

(54) Ibach, H.; Lüth, H. *Solid State Physics: An Introduction to Principles of Material Sciences*; Springer: Berlin, 2009.

(55) Botti, S.; Andreani, L. C. Electronic States and Optical Properties of GaAs/AlAs and GaAs/Vacuum Superlattices by the Linear Combination of Bulk Bands Method. *Phys. Rev. B* **2001**, *63*, No. 235313.